This is a preprint, the final version is subject to change, of the American Mineralogist (MSA)
Cite as Authors (Year) Title. American Mineralogist, in press.
(DOI will not work until issue is live.) DOI: http://dx.doi.org/10.2138/am.2013.4341

Revision 1

Transformation of graphite to lonsdaleite and diamond in the Goalpara ureilite directly observed by TEM

Yoshihiro Nakamuta[1] and Shoichi Toh[2]

[1]University Museum, Kyushu University, Hakozaki, Fukuoka 812-8581, Japan
[2]HVEM Laboratory, Kyushu University, Motooka, Fukuoka 819-0395, Japan

ABSTRACT

Reflected-light microscopy and laser Raman spectroscopy of a polished thin section (PTS) of the Goalpara ureilite and x-ray powder diffraction (XRPD) analyses of the grains taken out of it elucidate the mode of occurrence of carbon grains which contain lonsdaleite and diamond in the Goalpara ureilite. The results enable us to get samples with which precise analyses can be made in order to know the formation mechanism of lonsdaleite and diamond in ureilites. Selected area electron diffraction (SAED) analyses and high resolution TEM (HRTEM) observations were carried out in the three unique directions of pristine graphite with two thin slices prepared from a carbon grain directly taken out of a PTS. SAED patterns reveal the relative crystal-axes orientations between graphite (Gr), lonsdaleite (Lo) and diamond (Di) as $(001)_{Gr}$ // $(100)_{Lo}$ // $(111)_{Di}$, $[210]_{Gr}$ // $[001]_{Lo}$ // $[2\text{-}1\text{-}1]_{Di}$ and $(1\text{-}20)_{Gr}$ // $(\text{-}120)_{Lo}$ // $(0\text{-}22)_{Di}$. The shapes of diffraction spots in the SAED patterns reveal that the transformation of graphite to lonsdaleite is initiated by sliding of hexagonal carbon planes of graphite along the [210] of graphite structure. These results suggest that lonsdaleite and diamond in ureilites formed directly from graphite through boat-type buckling and chair-type puckering of hexagonal carbon planes of graphite, respectively. The results of this study confirm the shock origin of diamond in ureilites.

Keywords: Ureilite, graphite, lonsdaleite, diamond, transformation mechanism, TEM

Revision 1

INTRODUCTION

Diamond was found in the Novo Urei meteorite, one of typical ureilites, first in meteorites in 1888 (Kunz, 1888). Lonsdaleite, hexagonal polymorph of diamond, was found in the Canyon Diablo iron and the Goalpara ureilite first in nature (Bundy and Kasper, 1967; Frondel and Marvin, 1967; Hanneman et al., 1967). So far, mineralogical properties of carbon minerals in ureilites have been only roughly determined by using acid-treatment residues because they exist in small quantities in ureilites (Hanneman et al., 1967; Le Guillou et al., 2010; Ringwood, 1960; Urey et al., 1957; Valter et al., 2003; Vdovykin, 1970). Then, the origin of diamonds in ureilites has been controversial (Arrhenius and Alfvén, 1971; Fukunaga et al., 1987; Lipschutz, 1964; Urey, 1956).

Berkley and Jones (1982) reported that euhedral graphite blades occur without diamond in the Allan Hills (ALH) 78019 ureilite. Euhedral tabular crystals of graphite were also found in the Nova 001 and Nullarbor 010 ureilites and hard lumps in graphite crystals were supposed to be diamond formed by shock (Treiman and Berkley, 1994). Nakamuta and Aoki (2000) investigated carbon minerals in very weakly and weakly shocked ureilites and observed blade-like shaped euhedral graphite crystals, being tan-grey color and bearing metallic luster, in the very weakly shocked ALH 78019 and Yamato (Y)-82100 ureilites with an optical microscope under a reflected light. They also observed blade-like shaped grains in weakly shocked ureilites, Kenna, Y-79158 and ALH 77257, although these grains are black in color and dull in luster. X-ray powder diffraction (XRPD) patterns of the grains directly picked up from the polished thin section (PTS) of the Kenna ureilite reveal that the grains are a mixture of graphite, compressed graphite and diamond. Lonsdaleite was not

found in these weakly shocked ureilites. The results suggest that diamond in ureilites was formed from well-crystallized graphite having euhedral shapes by shock. In order to confirm the origin of diamonds in ureilites and to elucidate the transformation mechanisms of graphite to lonsdaleite and diamond, direct observation of structures of graphite, lonsdaleite and diamond at the same area of a carbon grain is important but was not carried out until now. The Goalpara ureilite is one of heavily shocked ureilites and is known to contain lonsdaleite together with diamond (Hanneman et al., 1967). In this study, SAED analyses and HRTEM observations were carried out in three directions with two slices prepared from a carbon grain directly taken out of the PTS of the Goalpara ureilite and the transformation mechanisms from graphite to lonsdaleite and diamond were proposed.

MATERIALS AND EXPERIMENTAL METHODS

The Goalpara ureilite is a monomict ureilite (Papike, 1998; Vdovykin, 1970). Urey et al. (1957) found diamond in an acid-tretment residue of the meteorite based on an XRPD analysis. Lonsdaleite was also found in an acid-tretment residue of the meteorite by an XRPD analysis (Hanneman et al., 1967).

A PTS was prepared from a fragment of the Goalpara ureilite and observed by an optical microscope. The meteorite mainly composed of coarse-grained olivine and pigeonite with minor amounts of blade-like shaped carbon grains, being black in color and dull in luster under a reflected light and up to 0.5 mm in size. Olivine and pyroxene crystals partly show a mosaic texture, suggesting that the meteorite has been heavily shocked. Melting of silicate minerals was not observed.

Micro Raman spectra of carbon grains in the PTS were recorded with a Jobin-Yvon T64000 triple-grating spectrometer equipped with confocal optics and a nitrogen-cooled CCD detector. A microscope was used to focus the 514.5 nm Ar exitation laser beam to a 1 μm spot. Accumulations lasting 120 seconds were made. The laser power on the sample was 2 mW.

After micro Raman analyses, a typical carbon grain, a hundred μm in size, was removed from the PTS and mounted on a glass fiber of ~10 μm in diameter for an XRPD analysis using a 114 mm diameter Gandolfi camera (Gandolfi, 1967). A rotating anode x-ray generator with a Cr-anode, 0.2 x 2 mm fine-filament, and a V-filter was used as an x-ray source. The x-ray powder diffraction pattern was two-dimensionally recorded on an imaging plate (IP), 35 mm wide and 350 mm long, and the intensity data on IP were read by the 50 x 50 μm pixel size with a Fuji-film BAS-2500 IP-scanner. Intensities of diffracted x-rays for each Bragg angle were obtained at intervals of 0.025º (2θ) by averaging those along a Laue cone over 300 pixels of the central part of IP that had the width of about 560 pixels.

SAED and HRTEM analyses were performed by using two thin slices of about 150 nm thick which were prepared from the grain removed from a glass fiber used for the x-ray analysis. FIB sample preparation was performed with a Ga ion beam by Hitachi FB-2000K equipped with a micro-sampling unit at the Art, Science and Technology Center for Cooperative Research, Kyushu University. One of the sides of the rectangular-shaped slice, 10 x 10 μm in size, was attached to the chipped edge of a copper disk of 3 mm in diameter and set into TEM. SAED patterns and HRTEM imags were obtained by JEM-3200FSK

with a 300 kV accelerating voltage and a 400 mm camera length and recorded by a CCD camera at the Research Laboratory for High Voltage Electron Microscopy of Kyushu University. Diffraction patterns of Au were also obtained and used in order to correct *d*-values of reflections of carbon minerals.

RESULTS

The mode of occurrence of carbon grains

Carbon grains occur along the grain boundaries of olivine with blade-like shapes (Fig. 1a). The rims of olivine crystals in contact with carbon grains include many tiny metal blebs. The rims are thought to have been produced by redox reaction between olivine grains and carbon when the parent body of ureilites has been break up (Goodrich, 1992; Goodrich et al., 2004). The carbon grain, C1 in Figure 1a, was taken out of the PTS. The grain is platy in shape with a thickness of 20 μm and a width of 100 x 100 μm (Fig. 1b). The shape of the grain implies that the carbon grain has originally crystallized as a single crystal of graphite (Berkley and Jones, 1982; Nakamuta and Aoki, 2000; Treiman and Berkley, 1994).

Raman spectroscopy

Raman spectra were measured at twenty points selected at random on the surface of the C1 grain in the PTS (Fig. 1a). All spectra obtained are very similar to each other and show a very broad Raman band spreading over the positions between 1200 and 1650 cm^{-1} and high-fluorescence back ground (Fig. 2). The broad band has two peaks at around 1330 and

1590 cm^{-1}, which may correspond to one-phonon band of diamond at 1332 cm^{-1} and E_{2g} band of graphite at 1580 cm^{-1} (Hanfland et al., 1989), respectively.

XRPD analysis

An XRPD pattern was obtained by using the whole grain taken out of the PTS before digging a hole to take a slice for TEM analysis. The picture of the grain after digging a hole is shown in Figure 1b. The XRPD pattern (Fig. 3) reveals that the grain is composed of graphite, compressed graphite, lonsdaleite and diamond with minor amounts of clinoenstatite, kamacite and maghemite. As can be seen in Figure 1a, the grain is in contact with the reduction rim of a olivine crystal, which is thought to be composed of iron metal and magnesium pyroxene (Goodrich, 1992; Hezel et al., 2008). Then, clinoenstatite, kamacite and maghemite, a weathering product of kamacite (Lindsley, 1976), are thought to be a part of reduced rim of olivine and exist on the surface of the carbon grain. It is noticeable that the reflections of diamond are much broader than those of diamonds reported from weakly shocked ureilites (Nakamuta and Aoki, 2000). The broad reflections suggst that diamond in the Goalpara ureilite is smaller in a grain size and/or ill-crystallized than those from weakly shocked ureilites.

SAED analyses and HRTEM observations

Two thin slices, one parallel to and the other perpendicular to the flat surface of the platy grain, denoted by S1 and S2, respectively, were prepared by a FIB method. The relative orientation of the two slices and the directions of an electron beam, D1, D2 and D3, by

which SAED patterns were obtained are summarized in Figure 4. The sizes of the areas where SAED patterns were obtained are about 130 nm in diameter.

Figure 5 shows the SAED pattern obtained with the electron beam perpendicular to the flat surface of the grain, the D1 direction in Figure 4, and interpretation of the pattern. The pattern can be interpreted as resulting from a three-fold rotation of a lonsdaleite [210] single crystal pattern, however, one of the three [210] patterns is more intense than the other two and a diamond [111] single crystal pattern is superimposed on it.

The pattern in Figure 5 is similar to the electron diffraction pattern shown in Figure 1 of Wheeler and Lewis (1975), although reflections from diamond are much stronger than the pattern of this study. They interpreted their pattern as resulting from a three-fold rotation of a diamond [112] single crystal pattern. The atomic arrangements of diamond projected on the (112) plane of diamond are very similar to those of lonsdaleite projected on the (100) plane of lonsdaleite and it is impossible to distinguish between the lonsdaleite [210] and the diamond [112] patterns. Referred to the SAED patterns obtained with the electron beam in other directions (Figs. 6 and 9), the interpretation shown in Figure 5 is thought to be reasonable.

Three SAED patterns in Figure 6 were obtained with an electron beam in the same direction parallel to the flat surface of the grain, the D2 direction in Figure 4, but at the different areas of the S2 slice. All these patterns can be interpreted as overlapped patterns of graphite [210], lonsdaleite [001] and diamond [2-1-1] single crystals but **a**, **b** and **c** patterns differ from each other in being dominated by reflections from graphite, lonsdaleite and diamond, respectively. The crystal axes orientations of graphite, lonsdaleite and diamond in

158 the carbon grain obtained with the S2 slice are consistent with those obtained with the S1
159 slice (Fig. 5), although S1 and S2 slices were prepared from the different areas of the
160 carbon grain. The consistent orientations in two slices strongly suggest that pristine
161 graphite was a single crystal or twinned crystals of which *c*-axes were perpendicular to the
162 flat surface of the grain. These SAED patterns clearly suggest the following relative crystal-
163 axes orientation between graphite (Gr), lonsdaleite (Lo) and diamond (Di): $(001)_{Gr}$ //
164 $(100)_{Lo}$ // $(111)_{Di}$, $[210]_{Gr}$ // $[001]_{Lo}$ // $[2\text{-}1\text{-}1]_{Di}$ and $(1\text{-}20)_{Gr}$ // $(\text{-}120)_{Lo}$ // $(0\text{-}22)_{Di}$. The
165 relative crystallographic orientation is shown in the drawings of the structures of 2H-
166 graphite, lonsdaleite and diamond (Fig. 7). It is also noticeable in Figure 6a that the
167 reflection from (1-20) of graphite is stronger than the calculated one and is elongated along
168 the *c**-axis of graphite. The elongation of the spots is thought to have occurred as an effect
169 of shock and discussed later.

170 In order to know the distribution of graphite, lonsdaleite and diamond in the grain, dark
171 field images of a part of the S2 slice were obtained together with a bright field image (Fig.
172 8). The image of Figure 8b was made by combining four dark field images and purple,
173 orange and red areas are thought to correspond to the areas mainly occupied by graphite,
174 lonsdaleite and diamond, respectively. The blue area does not correspond to a specific
175 carbon mineral and is thought to correspond to the disordered structure intermediate
176 between graphite and lonsdaleite or diamond. Figure 8b reveals that domains mainly
177 composed of graphite, lonsdaleite or diamond exist in the grain with a complex mosaic
178 texture. The mode of occurrence of graphite, existing as laminated domains surrounded by
179 diamond or lonsdaleite, reveals that graphite in the grain is not a back inversion product of

diamond but pristine one. The lack of melting in the neighboring silicates also strongly suggests that the post-shock temperature was not high enough to induce diamond-graphite back inversion.

Stacking sequence of diamond can be observed in the [10-1] direction of diamond, being at an angle of 30° relative to [2-1-1] direction (Fig. 7c). Then, the S2 slice was also observed in the D3 direction in Figure 4 after rotating the sample 30° relative to the direction at which the SAED patterns of Figure 6 were obtained. The SAED patterns are shown in Figure 9. The SAED pattern **a** can be interpreted as that from a diamond single crystal of which [10-1] is parallel to an electron beam as indices of reflections are shown in **b**. In the pattern, however, the reflections from {020}, {004}, {202} and {222} appear which are forbidden for diamond with Fd3m symmetry. It is also noticeable that the intensity of 1-11 reflection is a little stronger than that of 111 reflection and the *d*-spacing of 1-11, 0.203 nm, is smaller than that of 111, 0.208 nm.

The 111 reflection of diamond observed in the pattern of Fig. 9a can be the result of overlapping of reflections from three single crystals of diamond related by the three-fold rotation axis, as the [111] direction of diamond is parallel to the three-fold rotation axis of original graphite (Fig. 7). However, the 1-11 reflection can not be the result of such overlapping of reflections. Then, the fact that the 1-11 reflection is stronger than the 111 reflection cannot be explained by overlapping of reflections from twinned crystals and is thought to be intrinsic together with the difference in *d*-spacing. HRTEM image of diamond giving the pattern of Figure 9a is shown in Figure 10 together with the structure corresponding to it. In the image, (020) lattice fringes, having 0.18 nm spacing, are also

observed together with (111) and (1-11) fringes, having 0.21 nm spacing. The HRTEM image confirms the deviation of the structure from diamond with Fd3m symmetry.

The SAED pattern of Figure 9c is obtained in the same direction as Figure 9a but at a different area of S2. The diffraction spots in the pattern can be interpreted as those from two twin individuals of diamond related to the spinel twin law. Forbidden reflections for diamond also appear, however, different from that of Figure 9a, the *d*-spacing of 1-11 reflection, 0.208 nm, and its intensity do not differ from that of 111 reflection. Then, the structure is thought not to deviate from diamond and the forbidden reflections may be due to double reflections. In addition, the SAED pattern shows additional spots cutting the main diffraction spots by one-third along the [111] direction. These reflections are interpreted as by double reflections due to twinning on the (111) plane (Yusa et al., 1998).

DISCUSSION

Transformation mechanisms of graphite to lonsdaleite and diamond

SAED patterns obtained in this study clearly suggest the following relative crystal-axes orientation between graphite (Gr), lonsdaleite (Lo) and diamond (Di):
$(001)_{Gr}$ // $(100)_{Lo}$ // $(111)_{Di}$, $[210]_{Gr}$ // $[001]_{Lo}$ // $[2\text{-}1\text{-}1]_{Di}$ and $(1\text{-}20)_{Gr}$ // $(\text{-}120)_{Lo}$ // $(0\text{-}22)_{Di}$. The relative crystallographic orientation is shown in the drawings of the structures of 2H-graphite, lonsdaleite and diamond in Figure 7. It is also noticeable that the reflections from (1-20) of graphite in Figure 6a is stronger than the calculated one and is elongated along the *c**-axis of graphite.

As can be seen in Figure 7, if the hexagonal carbon planes of lonsdaleite and diamond are stretched, the AB′-sequence of lonsdaleite can be derived from 2H-graphite by sliding alternate planes by about 0.07 nm (Scandolo et al., 1995; Takano et al., 1991), and the ABC-sequence of diamond by sliding every third plane by about 0.14 nm, along the [210] direction of 2H-graphite.

The elongation of the reflection from (1-20) of graphite along the *c**-axis in Figure 6a can be assigned to the stacking fault of atom-planes which are vertical to the *c**-axis (Wilson, 1962). The strong intensity of this reflection also suggests that the (1-20) atom-planes were not disturbed by the stacking fault, i.e., stacking fault was formed by sliding parallel to (1-20) atom-planes of graphite. Then, it is reasonable to think that sliding of hexagonal carbon planes of graphite toward the direction parallel to [210] of pristine graphite occurred and AB'-stacking of lonsdaleite and ABC-stacking of diamond have formed. The 2H-stacking of graphite has been also found to change to ABC-stacking by grinding (Bacon, 1950) or by pressing at a high-pressure (Naka et al., 1976; Zhao and Spain, 1989). These results suggest that stacking change of 2H-graphite is not so difficult to occur and support the results of this study.

Lonsdaleite and diamond structures can be produced after such sliding through boat-type buckling and chair-type puckering of hexagonal carbon planes, respectively (Fahy et al., 1986; Lonsdale, 1971). In the pattern of diamond shown in Figure 9a, the reflections from {020}, {004}, {202} and {222}, which are forbidden for diamond, appear. The HRTEM image of diamond giving the pattern of Figure 9a also shows (020) lattice fringes together with (111) and (1-11) fringes. These observations reveal that the crystal has a structure

deviated from diamond which bears the Fd3m symmetry. As can be seen in Figure 10b, in the puckering process of graphite to diamond, C-C bonding which interconnects (111) atom planes forms by replacing π-bonding between hexagonal carbon planes of graphite, but C-C bonding which interconnects (1-11) atom planes forms through breaking sp^2-bonding of hexagonal carbon planes. In the intermediate or imperfectly puckered state of the transformation from graphite to diamond, the kinetic difference between (111) and (1-11) planes of diamond may cause a deviation of structure from diamond as revealed by the SAED pattern of Figure 9a.

The appearance of forbidden reflections was also noticed for diamonds synthesized at high-temperatures and high-pressures (Endo et al., 1994; Hirai and Kondo, 1991) and Hirai and Kondo (1991) thought it to be a modified form of diamond and called it n-diamond. So far, the structure of n-diamond has not been determined, however, is presumed to be intermediate one between the rhombohedral graphite and the cubic diamond, in which hexagonal carbon planes are stacked by an ABC-sequence with only about 0.207 nm interplanar distance but the carbon planes are near to planar with less puckering than observed in diamond structure (Hirai et al., 1992; Wen et al., 2006). The presumed structure of n-diamond as an intermediate one between rhombohedral graphite and diamond is in harmony with the results of this study.

Figure 11 is a plot of *a* and *c* lengths of lonsdaleite determined from the SAED patterns taken with an electron beam perpendicular to the flat surface of the carbon grain as shown in Figure 5. In Figure 11, *a* and *c* lengths of the ideal lonsdaleite (Bundy and Kasper, 1967) and corresponding dimensions of graphite with AB'-stacking of planar hexagonal carbon

267 planes (AB'-graphite) were also plotted. Lonsdaleites of this study have a little smaller *a*
268 and a little larger *c* dimensions than those of the ideal lonsdaleite and are plotted on the line
269 joining ideal lonsdaleite and AB'-graphite. These results suggest that buckling of the
270 hexagonal carbon planes in lonsdaleite of this study is in an intermediate or an imperfect
271 state as in the case of diamond showing forbidden reflections. The appearance of forbidden
272 004 reflection of lonsdaleite observed in Figure 5a may be due to such deviation of the
273 structure.

274 Single crystal graphite is known to transform to a transparent high-pressure phase at 18
275 GPa and at room temperature (Utsumi and Yagi, 1991). But the high-pressure phase formed
276 at room temperature is unquenchable upon the release of pressure. The crystal structure of
277 the high-pressure phase formed at room temperature is controversial (Mao et al., 2003;
278 Miller et al., 1997; Wang et al., 2011; Yagi et al., 1992). Yagi et al. (1992) showed in their
279 high-pressure *in situ* x-ray diffraction study that x-ray diffraction profiles of the phase are
280 well explained by lonsdaleite structure and the orientational relation is the same as that of
281 graphite and lonsdaleite. The *a* and *c* lengths of the phase determined by Yagi et al. (1992)
282 are also plotted in Figure 11 (open square). The transparent high-pressure phase is plotted at
283 a point near the area of lonsdaleite of this study. These results strongly suggest that the
284 transparent high-pressure phase has an intermediate structure between AB'-graphite and
285 lonsdaleite in which sp^3 connections between adjacent hexagonal carbon planes are
286 partially formed (Miller et al., 1997).

287 In order to make boat-type connections with adjacent planes, hexagonal carbon planes in
288 AB'-graphite have to bend sharply as can be seen in Figure 7 in contrast to moderate

289 corrugation of hexagonal carbon planes in diamond structure. Tateyama et al. (1996)
290 showed in their constant-pressures first-principles calculations that the activation barrier
291 from graphite to lonsdaleite is higher than that to diamond by about 70 meV/atom. This
292 high activation barrier for lonsdaleite is due to large out-of-plane movement of atoms in
293 order to make boat-type connections. If an intermediate structure between AB'-graphite and
294 lonsdaleite was formed the structure should bear high internal strain energy due to the
295 bended hexagonal carbon planes. Then, in order to keep lonsdaleite structure after the
296 release of pressure, the domains having sp^3 connections between adjacent hexagonal carbon
297 planes are necessary to develop larger than a critical size. The growth of the domains larger
298 than the critical size may be attained at higher temperature than the setting temperature
299 proposed by Bundy and Kasper (1967).
300 The AB'-sequence of lonsdaleite can be derived from 2H-graphite by sliding alternate
301 planes by about 0.07 nm and the ABC-sequence of diamond by sliding every third plane by
302 about 0.14 nm, twice for AB'-sequence of lonsdaleite. Then, it is reasonable to think that if
303 the collective slide of carbon planes is allowed, diamond which bears the lower activation
304 barrier than lonsdaleite will from. When the collective slide is inhibited, due to a large
305 crystal size or other reasons (Tateyama et al., 1996), lonsdaleite is expected to occur, as in
306 the case of this study and the synthesis by Bundy and Kasper (1967).
307

308 **Origin of graphite, lonsdaleite and diamond in ureilites**

309 Euhedral tabular crystals of graphite suggesting igneous origin were found in very weakly
310 shocked ureilites (Berkley and Jones, 1982; Nakamuta and Aoki, 2000; Treiman and

311 Berkley, 1994). The tabular shape of the carbon grain analyzed in this study suggests that
312 the carbon grain before transformation was a single crystal or twined crystals of graphite of
313 which *c*-axes were perpendicular to the flat surface of the grain. The crystal-axes
314 orientations of graphite, lonsdaleite and diamond which are consistent in two slices
315 prepared from different areas of the carbon grain support that lonsdaleite and diamond
316 formed from a single crystal or twined crystals. Then, it is reasonable to think that well-
317 crystallized graphite coexisted with olivine and pyroxene during igneous processes
318 (Goodrich et al., 2004) was converted to lonsdaleite or diamond by impact (Nakamuta and
319 Aoki, 2000).
320

321 **ACKNOWLEDGMENTS**

322 We thank M. Matsui for improvement of the manuscript, N. Kuwano for permission to
323 use the Hitachi FB-2000K for an FIB method and T. Aoki for assistance in the preparation
324 of TEM samples by FIB. We thank Oliver Tschauner (Associate Editor) and two
325 anonymous referees for the constructive comments that have helped to improve the overall
326 quality of our paper.
327

328 **REFERENCES CITED**

329 Arrhenius, G. and Alfvén, H. (1971) Fractionation and condensation in space. Earth and
330 Planetary Science Letters, 10, 253-267.
331 Bacon, G.E. (1950) A note on the rhombohedral modification of graphite. Acta
332 Crystallographica, 3, 320.

333 Berkley, J.L. and Jones, J.H. (1982) Primary igneous carbon in ureilites: Petrological
334 implications. Journal of Geophysical Research, 87, A353-A364.
335 Bundy, F.P. and Kasper, J.S. (1967) Hexagonal diamond - A new form of carbon. The
336 Journal of Chemical Physics, 46, 3437-3446.
337 Endo, S., Idani, N., Oshima, R., Takano, K.J., and Wakatsuki, M. (1994) X-ray diffraction
338 and transmission-electron microscopy of natural polycrystalline graphite recovered
339 from high pressure. Physical Review B, 49, 22-27.
340 Fahy, S., Louie, S.G., and Cohen, M.L. (1986) Pseudopotential total-energy study of the
341 transition from rhombohedral graphite to diamond. Physical Review B, 34, 1191-
342 1199.
343 Frondel, C. and Marvin, U.B. (1967) Lonsdaleite, a hexagonal polymorph of diamond.
344 Nature, 214, 587-589.
345 Fukunaga, K., Matsuda, J., Nagao, K., Miyamoto, M., and Ito, K. (1987) Noble-gas
346 enrichment in vapour-growth diamonds and the origin of diamonds in ureilites.
347 Nature, 328, 141-143.
348 Gandolfi, G. (1967) Discussion upon methods to obtain x-ray <<powder patterns>> from a
349 single crystal. Mineralogica et Petrographica Acta, 13, 67-74.
350 Goodrich, C.A. (1992) Ureilites: A critical review. Meteoritics, 27, 327-352.
351 Goodrich, C.A., Scott, E.R.D., and Fioretti, A.M. (2004) Ureilitic breccias: Clues to the
352 petrologic structure and impact disruption of the ureilite parent asteroid. Chemie der
353 Erde - Geochemistry, 64, 283-327.
354 Hanfland, M., Beister, H., and Syassen, K. (1989) Graphite under pressure: Equation of

355 state and first-order Raman modes. Physical Review B, 39, 12598-12603.
356 Hanneman, R.E., Strong, H.M., and Bundy, F.P. (1967) Hexagonal diamonds in meteorites:
357 Implications. Science, 155, 997-999.
358 Hezel, D.C., Dubrovinsky, L., Nasdala, L., Cauzid, J., Simionovici, A., Gellissen, M., and
359 Schönbeck, T. (2008) In situ micro-Raman and X-ray diffraction study of diamonds
360 and petrology of the new ureilite UAE 001 from the United Arab Emirates.
361 Meteoritics and Planetary Science, 43, 1127-1136.
362 Hirai, H. and Kondo, K.I. (1991) Modified phases of diamond formed under shock
363 compression and rapid quenching. Science, 253, 772-774.
364 Hirai, H., Kondo, K.I., and Sugiura, H. (1992) Possible structural models of n-diamond: A
365 modified form of diamond. Applied Physics Letters, 61, 414-416.
366 Kunz, G.F. (1888) Diamonds in meteorites. Science, 11, 118-119.
367 Le Guillou, C., Rouzaud, J.N., Remusat, L., Jambon, A., and Bourot-Denise, M. (2010)
368 Structures, origin and evolution of various carbon phases in the ureilite Northwest
369 Africa 4742 compared with laboratory-shocked graphite. Geochimica et
370 Cosmochimica Acta, 74, 4167-4185.
371 Lindsley, D.H. (1976) The crystal chemistry and structure of oxide minerals as exemplified
372 by the Fe-Ti oxides. In: D. Rumble, Ed., Oxide Minerals. Reviews in Mineralogy,
373 Mineralogical Society of America, Washinton, D. C.
374 Lipschutz, M.E. (1964) Origin of diamonds in the ureilites. Science, 143, 1431-1434.
375 Lonsdale, K. (1971) Formation of lonsdaleite from single crystal graphite. American
376 Mineralogist, 56, 333-336.

377 Mao, W.L., Mao, H.K., Eng, P.J., Trainor, T.P., Newville, M., Kao, C.C., Heinz, D.L., Shu,
378 J., Meng, Y., and Hemley, R.J. (2003) Bonding changes in compressed superhard
379 graphite. Science, 302, 425-427.
380 Miller, E.D., Nesting, D.C., and Badding, J.V. (1997) Quenchable transparent phase of
381 carbon. Chemistry of Materials, 9, 18-22.
382 Naka, S., Horii, K., Takeda, Y., and Hanawa, T. (1976) Direct conversion of graphite to
383 diamond under static pressure. Nature, 259, 38-39.
384 Nakamuta, Y. and Aoki, Y. (2000) Mineralogical evidence for the origin of diamond in
385 ureilites. Meteoritics and Planetary Science, 35, 487-493.
386 Mittlefehldt, D.W., McCoy, T.J., Goodrich, C.A., and Kracher, A. (1998) Non-chondritic
387 meteorites from asteroidal bodies. In J.J. Papike, Ed., Planetary Materials. Reviews
388 in Mineralogy, Mineralogical Society of America, Washington, D. C.
389 Ringwood, A.E. (1960) The Novo Urei meteorite. Geochimica et Cosmochimica Acta, 20,
390 1-4.
391 Scandolo, S., Bernasconi, M., Chiarotti, G.L., Focher, P., and Tosatti, E. (1995) Pressure-
392 induced transformation path of graphite to diamond. Physical Review Letters, 74,
393 4015-4018.
394 Takano, K.J., Harashima, H., and Wakatsuki, M. (1991) New high-pressure phases of
395 carbon. Japanese Journal of Applied Physics, 30, 860-863.
396 Tateyama, Y., Ogitsu, T., Kusakabe, K., and Tsuneyuki, S. (1996) Constant-pressure first-
397 principles studies on the transition states of the graphite-diamond transformation.
398 Physical Review B, 54, 14994-15001.

399 Treiman, A.H. and Berkley, J.L. (1994) Igneous petrology of the new ureilites Nova 001
400 and Nullarbor 010. Meteoritics, 29, 843-848.
401 Urey, H.C. (1956) Diamonds, meteorites, and the origin of the solar system. The
402 Astrophysical Journal, 124, 623-637.
403 Urey, H.C., Mele, A., and Mayeda, T. (1957) Diamonds in stone meteorites. Geochimica et
404 Cosmochimica Acta, 13, 1-4.
405 Utsumi, W. and Yagi, T. (1991) Light-transparent phase formed by room-temperature
406 compression of graphite. Science, 252, 1542-1544.
407 Valter, A.A., Oleynik, H.S., Fisenko, A.V., and Semenova, L.F. (2003) Structural and
408 morphological evidence of the impact-induced development of diamond after
409 graphite in the Novo-Urei meteorite. Geochemistry International, 41, 939-946.
410 Vdovykin, G.P. (1970) Ureilites. Space Science Reviews, 10, 483-510.
411 Wang, J.T., Chen C., and Kawazoe, Y. (2011) Low-temperature phase transformation from
412 graphite to sp^3 orthorhombic carbon. Physical Review Letters, 106, 075501.
413 Wen, B., Zhao, J., Li, T., and Dong, C. (2006) N-diamond: An intermediate state between
414 rhombohedral graphite and diamond? New Journal of Physics, 8, 62-71.
415 Wheeler, E.J. and Lewis, D. (1975) The structure of a shock-quenched diamond. Materials
416 Research Bulletin, 10, 687-693.
417 Wilson, A.j.C. (1962) X-ray optics. 147 p. Methuen & Co Ltd, London.
418 Yagi, T., Utsumi, W., Yamakata, M.A., Kikegawa, T., and Shimomura, O. (1992) High-
419 pressure in situ x-ray-diffraction study of the phase transformation from graphite to
420 hexagonal diamond at room temperature. Physical Review B, 46, 6031-6039.

421 Yusa, H., Takemura, K., Matsui, Y., Morishima, H., Watanabe, K., Yamawaki, H., and Aoki,
422 K. (1998) Direct transformation of graphite to cubic diamond observed in a laser-
423 heated diamond anvil cell. Applied Physics Letters, 72, 1843-1845.
424 Zhao, Y.X. and Spain, I.L. (1989) X-ray diffraction data for graphite to 20 GPa. Physical
425 Review B, 40, 993-997.
426

Figure captions

FIGURE 1. (**a**) Reflected light view of carbon grains in a PTS. C1 and C2 are carbon grains. (**b**) C1 grain after extraction from the polished thin section and digging a hole to take a slice for TEM analyses.

FIGURE 2. Representative Raman spectrum of C1 grain. The Raman spectrum was obtained with a 514 nm Ar excitation laser beam under a microscope with confocal optics.

FIGURE 3. X-ray powder diffraction pattern of the C1 whole grain obtained by using a Gandolfi camera with Cr Kα radiation. G, c-G, L, D, E, M and K denote the reflections from graphite, compressed graphite, lonsdaleite, diamond, clinoenstatite, maghemite and kamacite, respectively. Index of each reflection is also shown together with an abbreviation for graphite, lonsdaleite and diamond.

FIGURE 4. A brief sketch showing the directions of an electron beam by which SAED patterns were obtained. S1 and S2 are the slices taken out of the carbon grain for TEM analyses. Arrows denoted by D1, D2 and D3 show the directions of an electron beam. D1 is perpendicular to the flat surface of the carbon grain. D2 and D3 are parallel to the flat surface of the carbon grain and are at an angle of 30° to each other.

FIGURE 5. SAED patterns of the carbon grain obtained with an electron beam perpendicular to the flat surface of the grain by using the S1 slice (**a**). (**b)** Explanation of the pattern. ○, × and ♦ are reflections from lonsdaleite, forbidden reflections for lonsdaleite

446 and reflections from diamond, respectively. Index of each reflection is also shown with
447 each symbol.

448 **FIGURE 6.** SAED patterns of the carbon grain obtained with an electron beam parallel to
449 the flat surface of the grain by using the S2 slice (**a**, **b**, **c**) and indexing (**d**). ○, ♦ and + in **d**
450 are reflections from lonsdaleite, diamond and graphite, respectively. Horizontal edges of
451 the photographs of the patterns are set parallel to the flat surface of the carbon grain. **a**, **b**
452 and **c** patterns are dominated by reflections from graphite, lonsdaleite and diamond,
453 respectively. It is also noticeable in **a** that the reflection from (1-20) of graphite is stronger
454 than the calculated one and is elongated along the *c**-axis of graphite.

455 **FIGURE 7.** Crystal structures of graphite (**a**), lonsdaleite (**b**) and diamond (**c**). The
456 structure of lonsdaleite consists of hexagonal carbon planes stacked with the AB'-sequence,
457 which buckle to form boat-type connections with adjacent planes. The structure of diamond
458 consists of hexagonal carbon planes stacked with the ABC-sequence, which pucker to form
459 chair-type connections with adjacent planes. In the lower figures, hexagonal carbon planes
460 A, B (B') and C are shown as dotted, broken and solid lines, respectively.

461 **FIGURE 8.** Bright field (**a**) and dark field (**b**) images of a part of the S2 slice. **b** was made
462 by combining four dark field images taken with the 002 reflection of graphite (purple), with
463 the 010 reflection of lonsdaleite (orange), with the overlapped reflections of lonsdaleite 100
464 and diamond 111 (red) and with the overlapped reflections of graphite 1-20, lonsdaleite -
465 120 and diamond 0-22 (blue). Referred to the intensities of reflections, purple, orange and

red areas are thought to correspond to the areas mainly occupied by graphite, lonsdaleite and diamond, respectively. The blue area does not correspond to a specific carbon mineral.

FIGURE 9. SAED patterns obtained after rotating the sample 30° relative to the direction at which the SAED patterns of Figure 6 were obtained (**a**, **c**). (**b**) Indexing of pattern **a**. ○ shows reflections from diamond and Δ shows forbidden reflections for diamond with Fd3m symmetry. (**d**) Interpretation of pattern **c**. Open symbols are the same as **b** and filled symbols are reflections from a twinned crystal related by spinel twin law. Crosses indicate the satellites by twinning.

FIGURE 10. HRTEM image of the crystal showing the SAED pattern of Figure 9a (**a**) and the diamond structure corresponding to it (**b**). Dotted lines in **b** show sp^3-bonding formed by replacing π-bonding between hexagonal carbon planes of graphite. Broken lines show sp^3-bonding formed through breaking sp^2-bonding of hexagonal carbon planes. (111), (1-11) and (010) atom planes are also shown.

FIGURE 11. Plot of *a* and *c* lengths of lonsdaleite determined from the SAED patterns as shown in Figure 5 by using the least squares method. Error bars in the plot show standard deviations. Ideal lonsdaleite, corresponding dimensions of AB'-graphite and transparent high-pressure phase of graphite (Yagi et al., 1992) are also plotted.

Figure 1

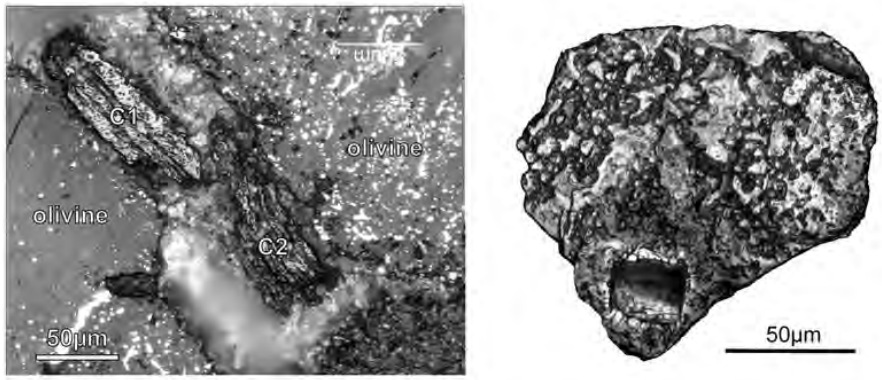

(a) (b)

Figure 2

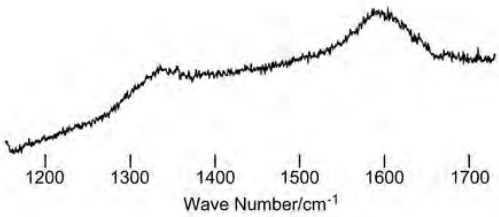

Figure 3

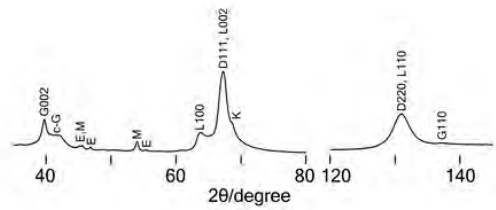

Figure 4

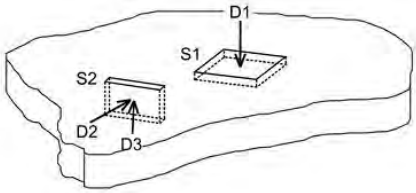

Figure 5

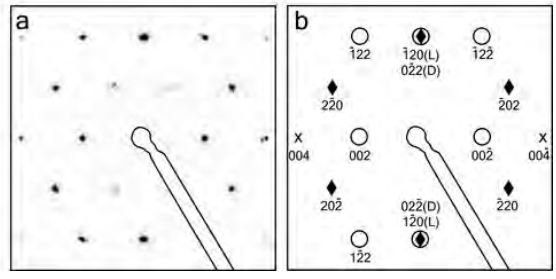

Figure 6

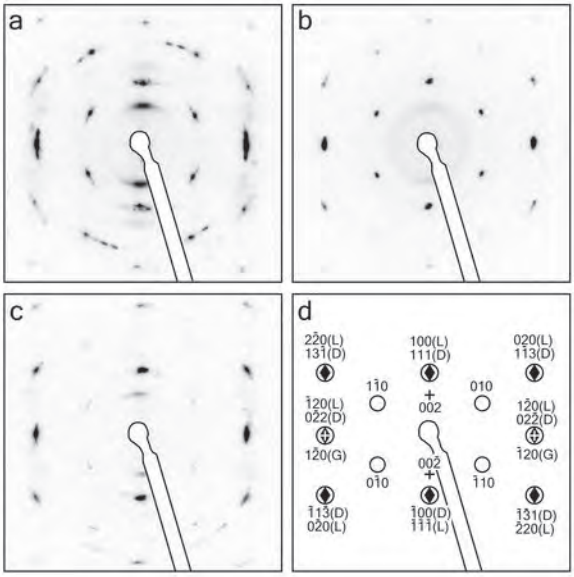

Figure 7

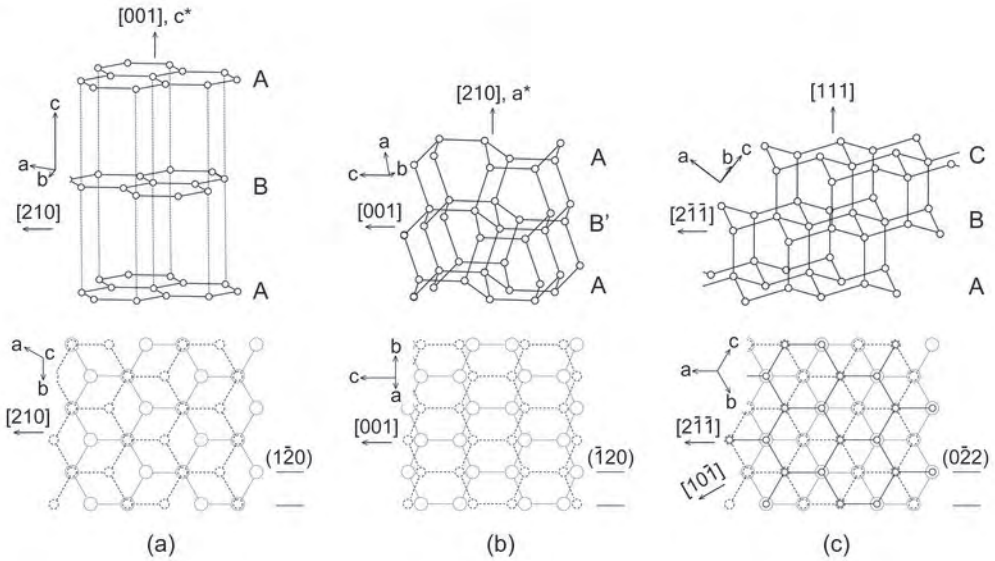

Figure 8

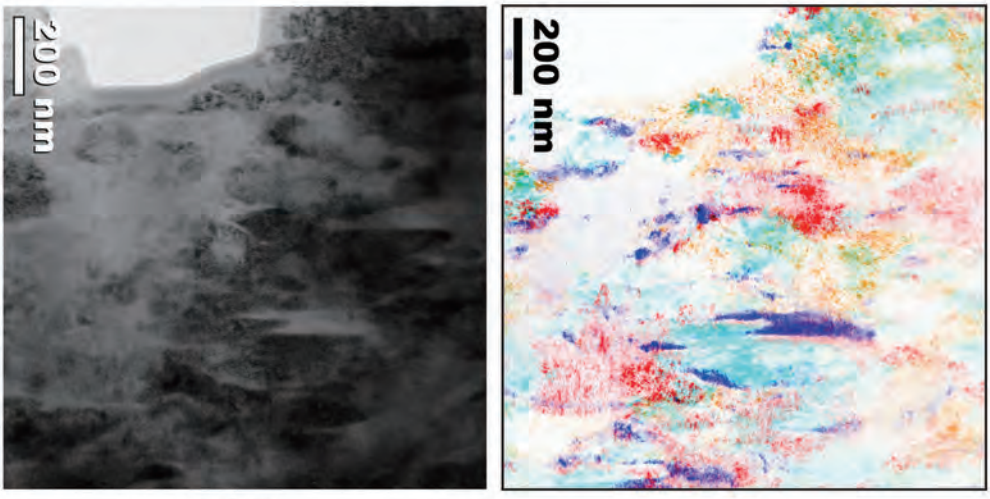

Figure 9

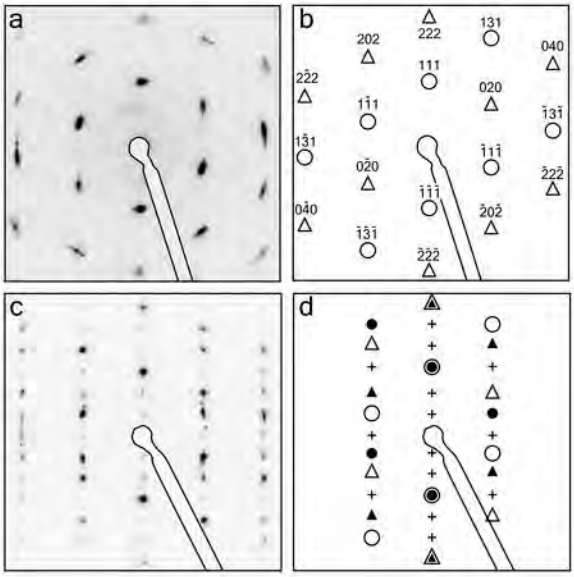

Figure 10

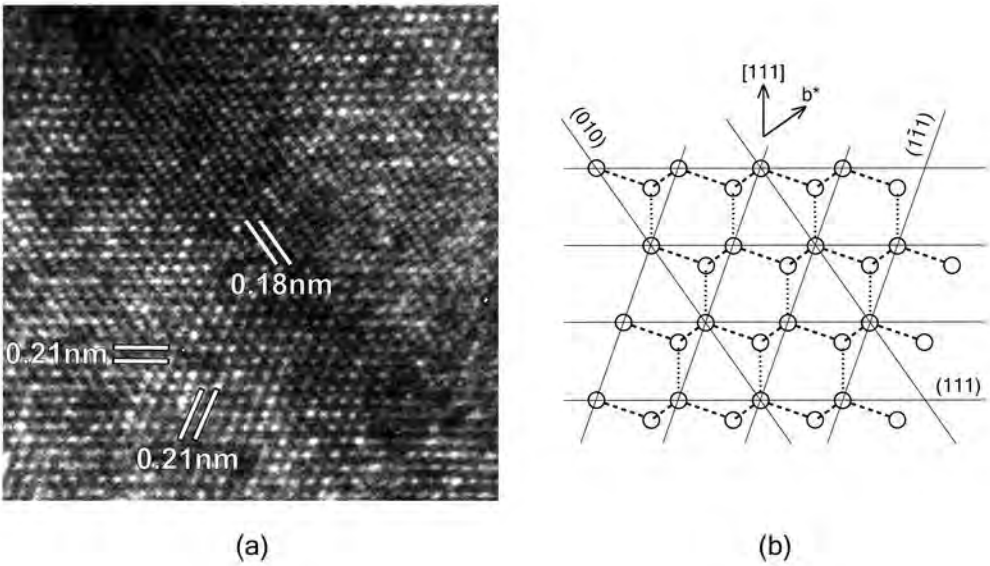

Figure 11